CONF-8909216--3

RLA VERTICAL TURNING FIELD DESIGN*

J. R. Freeman
Plasma Theory Division
Sandia National Laboratories
P. O. Box 5800
Albuquerque, NM 87185

SAND--89-2127C
DE90 001386

I. Introduction

The Recirculating Linear Accelerator (RLA) uses ion-focusing to provide the radial confinement of the beam. Fig. 1 shows the basic configuration of the RLA. At the ends of the ion-channel racetrack, a ramped vertical magnetic field will be required to keep the beam in the channel. A sector field, whose strength increases with distance from the channel axis, has been proposed [1-2] to provide an energy bandwidth for the transport system. This manuscript reports on design studies for coil systems that produce the required fields. It also describes particle simulations in the combined IFR-B-field transport system to address the issues of energy bandwidth and emittance growth.

II. Design of Magnetic Field Coils

The vertical field is to be produced by a 3-coil system shown schematically in Fig. 2. This configuration was suggested by David Hasti [3]. The radius of the turns is 2 m , much larger than the 5 cm drift tube radius. We have thus adopted a 2-D model for studying the fields, ignoring the curvature of the coils.

The RLA uses a stainless steel drift tube in the straight sections. One reason for the use of stainless steel is its attractive vacuum properties. In the bends, the stainless steel will carry induced currents that will reduce the bending field on the drift tube axis. This section reports on a numerical computation of the field distribution and comparisons with the fields produced for a non-conducting drift tube.

The bending fields must increase in time as the beam energy is increased by the accelerating gap. A typical ramp rate would have a 1 μs rise time. The magnetic skin depth in stainless steel would be 0.06 cm, much smaller than the wall thickness of 0.2 cm. This means that eddy currents will be induced on the drift tube walls, and that the field on-axis will be a superposition of the fields due to the coils and due to the image currents.

The magnetic field distribution was computed by solving for $\nabla^2 A_z = \mu_0 J_z$, assuming that σ_{wall} was infinite. An SOR finite difference solution was obtained on an r-θ mesh.

There are at least two ways to connect the coils to the electrical circuit that provides the coils current. In the first, all of the current supplied by the capacitor bank returns on the inner wall of the drift tube. The net current of the coils flows back in equal and opposite manner along the inner drift tube wall. The B-field inside of any perfect conductor is zero, and in this case, the B-field is zero outside as well.

The second way to connect the bank to the coils would use external current connections. The perfectly conducting drift tube wall is now electrically isolated, so that the equal and opposite current again flows on the inner drift tube wall, but in this case it must return on the outer surface of the drift tube wall. The B-field on-axis is the same as for the first case, but the B-field outside of the drift tube is now non-zero, decreasing with distance away from the drift tube. This means that the second method requires additional voltage and energy from the capacitor bank and is thus less efficient electrically.

The vector potential contours for the first method is shown in Fig. 3. The drift tube wall radius was 7 cm and the diameter of the current-carrying coils was 2.5 cm. The magnetic field is proportional to the spacing of these contour lines. The smallest spacing is seen to be between the coils and the drift tube, rather than on the axis where the beam will pass. This is thus an inefficient use of bank energy.

Fig. 4 plots vector potential contours for a case with perfectly resistive walls, such as glass or plastic. The magnetic field on-axis is about 1.75 X greater than that on-axis for the perfectly conducting wall case. In general, any wall material whose thickness could be much less than the skin depth would have similar results. The actual in-the-laboratory electrical efficiency of each of these two cases would depend on how the coils and the return leads are connected to the power source.

III. Particle Simulations for Transport System

A useful feature of the 3-wire coil configuration shown in Fig. 2 is that the vertical field near the axis approximates the field of a sector magnet. Specifically, the magnetic field varies as $B = B_0(r/R)^3$, where R is the radius of curvature and r measures the displacement of the beam from the axis, as shown in Fig. 5. This type of field profile has a larger energy bandwidth than a spatially uniform vertical magnetic field.

Beam electrons with larger γ have a larger centrifugal force and travel through the bend at a larger displacement r. If the B-field increases with r, these electrons can be confined to the drift tube. Fig. 6 plots B_y vs. x (or r) for a current of 1.3 kA in each coil, showing how B_y increases with r.

The beam dynamics were studied by particle simulations using the BUCKSHOT code [4]. The goal of the studies was to determine how a beam with a larger-than-matched γ would interact with the combined IFR-B-field transport system. The final beam radius,

divergence, particle loss, and emittance can be used to measure the energy bandwidth of the system.

The beam was injected onto the racetrack with an initial γ that was varied from a nominal value of eight to sixteen. The accelerating gap immediately increased γ by another eight. The sector magnetic fields were matched to the nominal $\gamma = 8$, and were ramped as γ increased. The initial beam and channel radii were 2.0 cm and f, the ratio of the channel line density to the beam line density was 1.0.

The gap model in BUCKSHOT assumed that $\beta_\perp\gamma$ was a constant, so that beam divergence $\beta_\perp$ (and emittance $\beta_\perp r_b$) was decreased by passage through the gap. The simulations were carried out for 3.25 circulations, the point at which the nominal beam would arrive at the extraction point with $\gamma = 40$. These runs used fixed ions to allow the study of emittance growth and particle loss due strictly to energy mismatch. A single slice of the beam, corresponding to the peak injected current of 10 kA, was modeled.

For the case with the mismatched injected $\gamma = 16$, the beam overshot the equilibrium orbit in the bend. Typical maximum rms offsets in the first bend were 0.7 cm (compared to a beam radius of 2 cm). This offset had phase-mix damped to 0.4 cm by the end of the back straight. The magnetic field in the the second bend was again too weak, allowing the maximum offset to increase back to 0.7 cm. The second circulation began after the accelerating gap had again increased the γ by eight, and had decreased the transverse velocity by $\gamma_{old}/\gamma_{new}$.

The process described above continued for the 3.25 circulations proposed for full RLA acceleration sequence. At the end of the simulation, the final rms beam radius and divergence were 1.75 cm and 0.1. This compares with values just after the first pass through the gap of $r_b = 2.1$ cm and $\beta_\perp = 0.17$. Comparisons of the final emittance values showed about a 25% increase over the matched case after accounting for the reduction due to the accelerating gap model. The particle loss to the drift tube wall was 25%, a marginal number. These runs suggest that the energy bandwidth of the IFR-B-field transport system will be less than 0.5 - 2.0 X the nominal γ. Substantial ion motion could reduce this bandwidth substantially.

A case was run for an energy mismatch more typical of the RLA. For $\gamma_{inj} = 6$ (compared to the nominal $\gamma_{inj} = 8$), the particle loss was only 2.5% and the final emittance was almost unchanged, save for a final offset equal to 5% of the beam radius.

IV. Summary

Three magnetic coil configurations were studied. These included a perfectly conducting wall carrying either zero net current or the coil return current. The third case employed a perfectly resistive wall. This latter case produced the highest field on axis per ampere of

coil current. The zero net current case was the least attractive option, as it had a reduced on-axis field and higher inductance than the non-zero wall net current case. The numerical methods developed for this work will be useful for studying the eventual laboratory configuration.

The computed 3-coil field distribution was used as input for a series of multi-circulation BUCKSHOT particle simulation runs. These runs were carried out to study the energy bandwidth of the transport system. Neglecting ion motion, the bandwidth is predicted to be less than 0.5-2.0 X the nominal γ.

References

1. D. E. Hasti, W. K. Tucker, S. L. Shope, K. R. Prestwich, R. B. Miller, and W. W. Rienstra, J. Def. Res., to be published, 1990.

2. W. Rienstra, "Theoretical and Computational Analysis of IFR Beam Transport on Curved Channels", Proc. 1987 IEEE Particle Accelerator Conf., Washington, D.C. (1987).

3. D. E. Hasti, private communication.

4. J. S. Wagner, "BUCKSHOT, a Gridless Magnetostatic Particle Code", Sandia National Laboratory Report SAND87-2019 (1989).

Acknowledgements

The author would like to acknowledge many helpful discussions with David Hasti. The version of the BUCKSHOT code used for this work was provided by John Wagner.

* This work was supported by the U.S. Department of Energy under Contract DE-AC04-76DP00789.

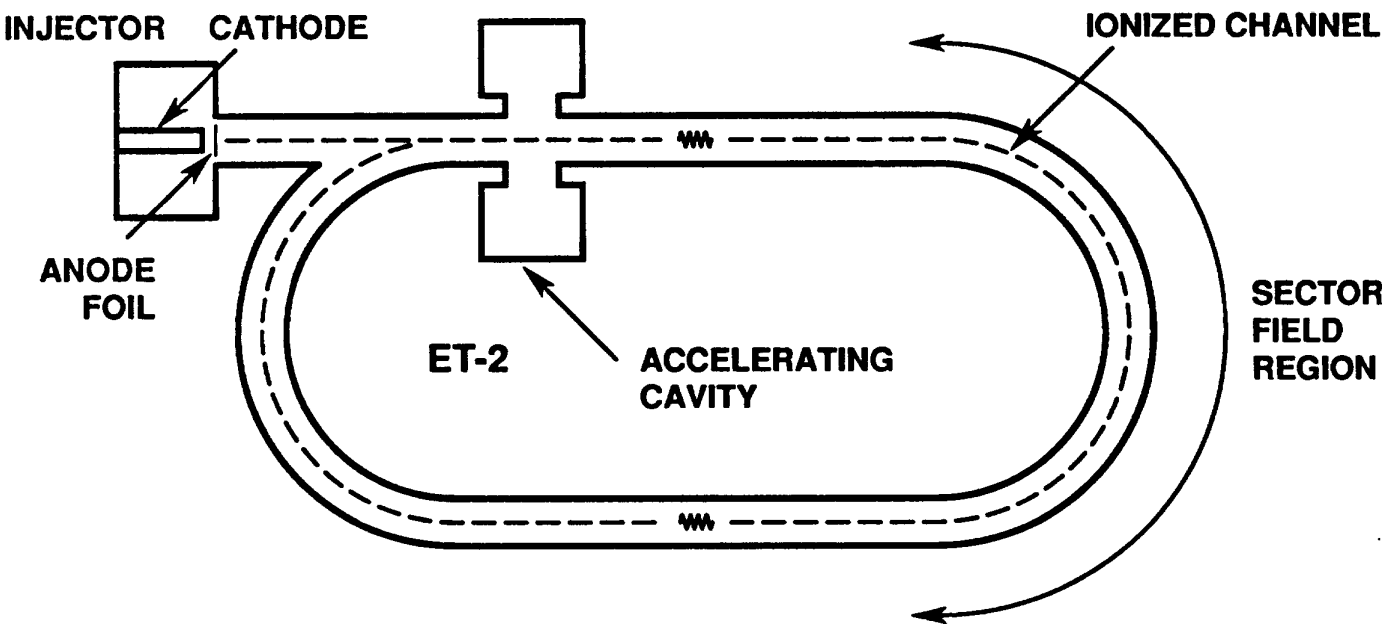

Figure 1. Schematic diagram of RLA.

TA0053.02.01

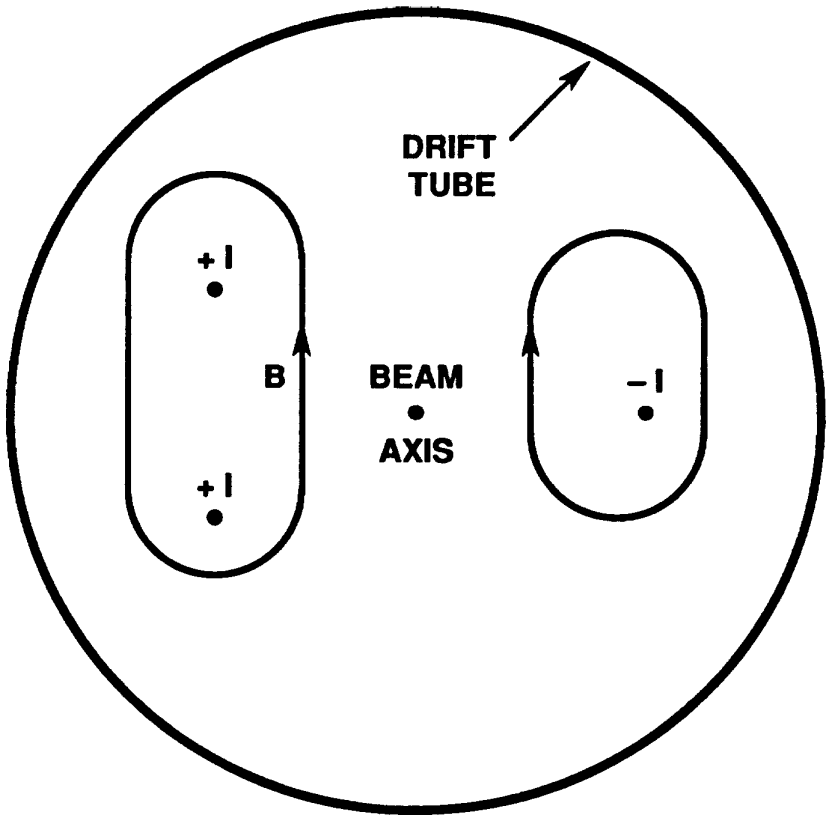

Figure 2. Coil configuration.

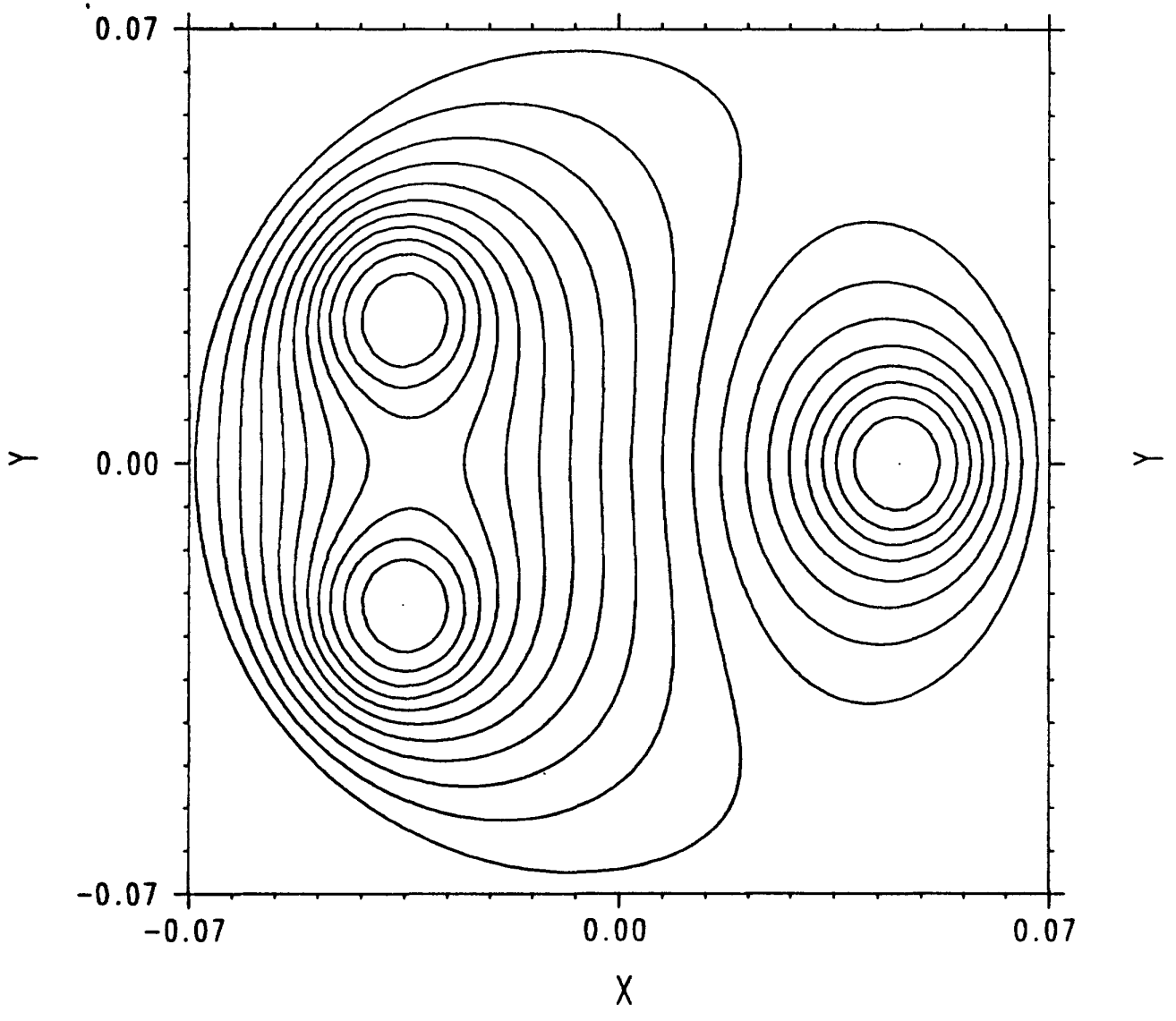

Figure 3. Vector potential contours, perfectly conducting wall.

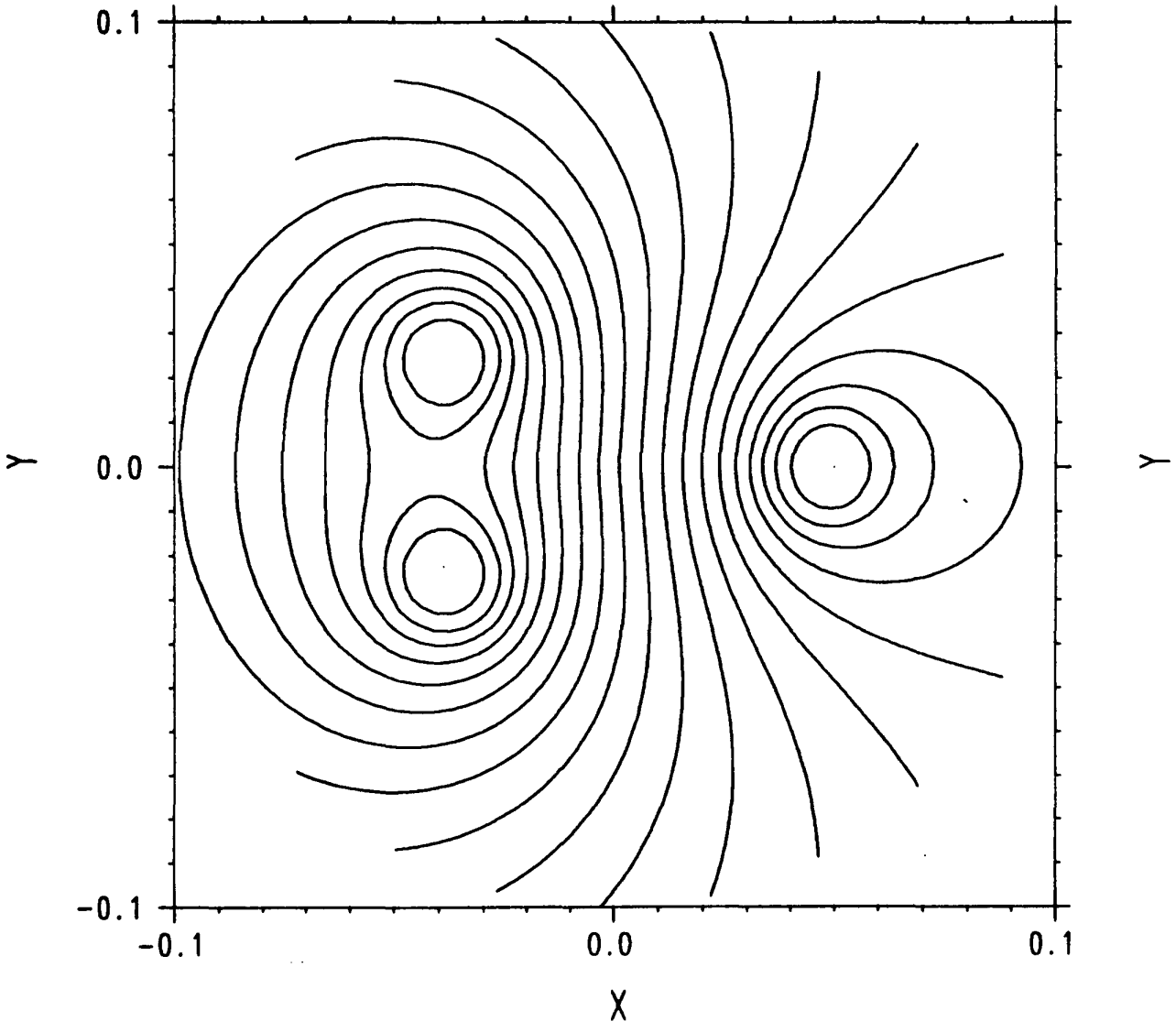

Figure 4. Vector potential contours, perfectly resistive wall.

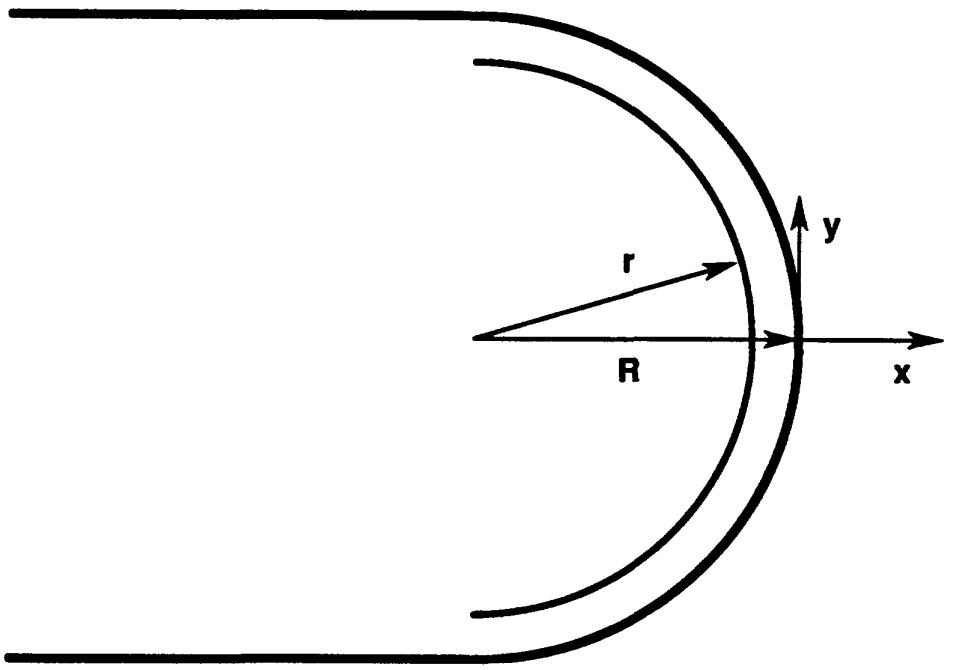

Figure 5. R is the radius of curvature of the racetrack.
r is the local radial coordinate.

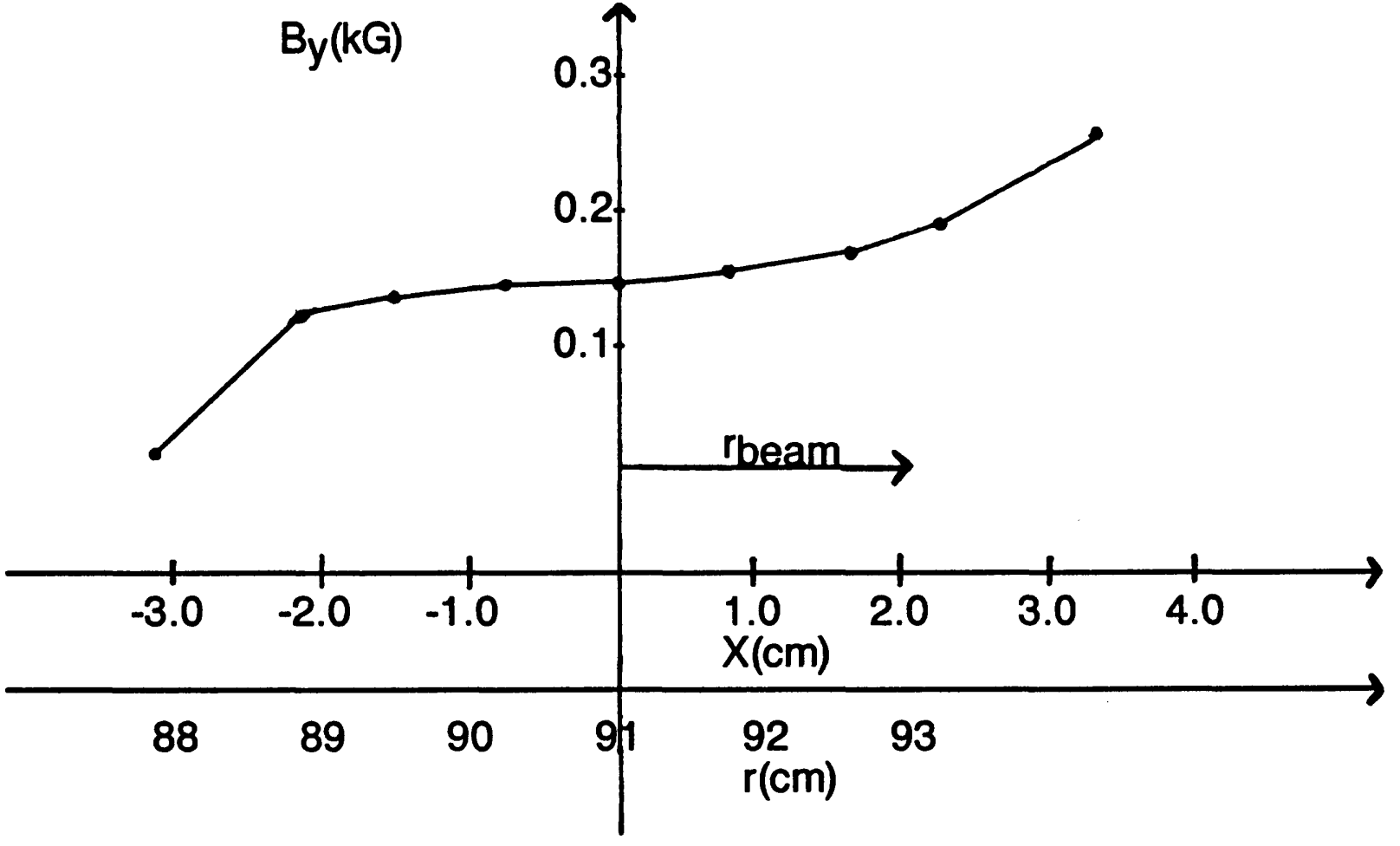

Figure 6. Vertical fields vs. major radius in racetrack.